

## Advanced oxidation Scanning Probe Lithography

Yu K. Ryu<sup>\*</sup> and Ricardo Garcia<sup>\*\*</sup>

Instituto de Ciencia de Materiales de Madrid, CSIC,  
c/ Sor Juana Inés de la Cruz 3, 28049 Madrid, Spain

<sup>\*</sup>Present address: IBM Zurich Research Laboratory, Säumerstrasse 4, 8803 Rüschlikon, Switzerland

<sup>\*\*</sup> email address: [r.garcia@csic.es](mailto:r.garcia@csic.es)

### Abstract

Force microscopy enables a variety of approaches to manipulate and/or modify surfaces. Few of those methods have evolved into advanced probe-based lithographies. Oxidation scanning probe lithography (o-SPL) is the only lithography that enables the direct and resist-less nanoscale patterning of a large variety of materials, from metals to semiconductors; from self-assembled monolayers to biomolecules. Oxidation SPL has also been applied to develop sophisticated electronic and nanomechanical devices such as quantum dots, quantum point contacts, nanowire transistors or mechanical resonators. Here, we review the principles, instrumentation aspects and some device applications of o-SPL. Our focus is to provide a balanced view of the method that introduces the key steps in its evolution, provides some detailed explanations on its fundamentals and presents current trends and applications. To illustrate the capabilities and potential of o-SPL as an alternative lithography we have favored the most recent and updated contributions in nanopatterning and device fabrication.

## 1. From atomic scale modifications to oxidation scanning probe lithography

The potential of scanning probe microscopes to modify or manipulate surfaces at atomic and nanometer scales was quickly recognized after the invention of the scanning tunneling microscope (STM) [1]. The combination of nanoscale patterning with the intrinsic metrology provided by probe microscopy generated an intense scientific activity. A paradigmatic example of single atom manipulation was provided by moving individual atoms of xenon on a nickel surface [2]. Atomic scale desorption and fragmentation was demonstrated on Si (111)7x7 surfaces in 1991 [3]. Since then, a large variety of approaches have been proposed and applied to either manipulate or modify surfaces in air, vacuum or liquid with atomic and nanometer-scale features [4-35].

A probe microscopy interface offers a variety of physical and chemical interactions to modify the surface of a material. Thermal interactions [5-11], bias-induced processes or reactions [12-14, 26], electrochemical reactions [19-23], thermally assisted catalytic reactions [24, 25], mechanical forces [16, 17] or the controlled deposition of ink molecules from the tip have been applied [15]. Those interactions or processes explain the emergence of a variety of probe-based methods for nanopatterning by either adding or removing material from the surface [29]. Three of the above processes have led to the development of specific scanning probe lithography methods (SPL), oxidation SPL [19], thermal SPL [8-10] and dip pen SPL [15].

In particular, oxidation SPL (o-SPL) has the following characteristics (Fig. 1). (a) It combines nanoscale patterning and device fabrication. (b) The method has a high degree of reproducibility in patterning sub-50 nm features. (c) The method can be scale up from the sub-10 nm domain to the micrometer domain. (d) It is compatible with other lithographic processes such as photolithography, electron beam lithography or physical etching. (e) Oxidation SPL experiments do not require ultra-high vacuum or at low temperature so the patterning or device fabrication process can be completed in a single day. (f) It can be applied to pattern a large variety of materials with relatively simplified processing protocols (Fig. 2). The above features make o-SPL a robust and widely used nanolithography in academic research [29]. The first o-SPL experiment was reported by Dagata and co-workers in 1990. They modified a hydrogen-terminated silicon surface with a STM operated in ambient air [4]. At about the same time, Thundat and co-workers used an STM to smooth tantalum surfaces [30]. In both cases a bias of a few volts was applied between the STM tip and sample surface. Secondary ion mass spectroscopy (silicon) and x-ray photoelectron spectroscopy (tantalum) showed that the modifications were due to the oxidation of the respective surfaces. The generality and robustness of the oxidation process have transformed the above observations into one of the most reliable and versatile probe-based lithography methods.

The local anodic oxidation or nano-oxidation method to modify surfaces has been improved and optimized through the years to become what is currently known as oxidation SPL [29]. The timelines represented in Fig. 2 show some of the key developments in instrumentation, material or devices that mark the evolution of o-SPL. The STM used in the first oxidation experiments was replaced by the atomic force microscope (AFM) as the main instrument to perform o-SPL [31, 33-35]. In fact, the replacement of the STM by the AFM has been a common feature in the development of robust and reliable probe-based patterning methods. The AFM is more suitable for lithography experiments because the feedback parameter that controls the imaging process, either a static cantilever deflection or its oscillation amplitude [36, 37], does not depend on the conductivity of the sample surface. A relevant feature of o-SPL is that the patterning and the

imaging processes operate independently. Long range van der Waals forces and/or short range repulsive forces are used to image the surface while an external voltage is applied to induce the local oxidation of the surface. In addition the AFM imaging modes allow *in situ* control of the device electric and topographic characteristics during its fabrication [38-39]. High resolution images of the sample can be obtained and used for precise alignment or assessment of the lithography without introducing further modifications on the fabricated nanostructures.

The capabilities of a force microscope devoted to o-SPL is not limited to produce local oxides. By changing the bias polarity or the gas composition it is possible to study a wide variety of different chemical or electrochemical processes in nanoscale volume. Those studies could be important in fields such as energy conversion and storage, catalysis or to fabricate novel electronic devices [40-43].

There is an extensive body of publications devoted to the development and/or applications of o-SPL. A partial account on o-SPL can be found in a recent and general review on SPL [29]. Similarly some reviews on tip-based modification processes provide some introductions to o-SPL [19, 21, 23, 31]. However, there is not a comprehensive review devoted to o-SPL. In this review we aim to provide a coherent and up-dated introduction to o-SPL principles and applications. We explain the role of the main factors that participate in the local anodic oxidation process, such as the water bridge and the voltage parameters. From the oxidation kinetics we describe the parameters that control the nanopattern size. We also introduce the main steps to perform an o-SPL experiment. The capabilities, achievements and potential of o-SPL are illustrated by reporting results in three lithographic areas: nanopatterning, template growth of nanostructures and nanoscale device fabrication.

## **2. Mechanism and kinetics of the patterning process**

Oxidation SPL is based on controlling the lateral and vertical extension of the anodic oxidation of a surface [19, 44, 45]. The oxidation reaction is driven by the application of a voltage bias between the AFM tip (negative) and the sample surface (positive) in the presence of oxyanions. Commonly the oxygen species are provided by a water bridge [46-48]. The strong localization of the electric field lines near the tip apex gives rise to a nanometer-size oxide dot. The term local comes from the smallness of the sample region that interacts with the end of a sharp tip. There are some similarities between the anodic oxidation process involved in o-SPL and conventional anodic oxidation [49]. The tip, the sample and the water bridge are the elements of a nanoscale electrochemical cell. The tip is the cathode, the sample is the anode and the water meniscus formed between tip and surface provides the oxyanions. The main difference between the o-SPL interface and a conventional electrochemical cell is the absence of a reference electrode.

### *2.1 The role of the water bridge*

The formation of a nanoscale water bridge connecting the tip and the sample is a key feature in o-SPL (Fig.1). Water molecules adsorbed on the surface and those coming from the gas phase contribute to the bridge [47]. The water bridge provides the oxygen species (mostly OH<sup>-</sup>) needed to oxidize the surface. It also confines spatially the oxidation reaction which in turns will define the size of the nanopattern. The spatial confinement depends on the geometry of the water bridge and the distribution of the electric field lines. The water bridge acts as an effective electrostatic lens which focuses the field lines within the water bridge limits [47, 50, 51]. The

focusing effect is enhanced by the differences in the electric permittivities inside and outside the liquid bridge, respectively, 81 and 1.

Molecular dynamic simulations have described the transformation of a water nanodroplet absorbed on a silicon surface into a nanoscale water bridge [52]. The formation of the water bridge is very fast. In the simulation it took 75 ps. The simulations show that the formation of a water bridge from a droplet requires a certain threshold value. The existence of a threshold value was previously observed experimentally [45,48].

### 2.2 The role of the bias voltage and the electric field

To drive the anodic oxidation process, the sample is positively biased with respect to the tip. The voltage or more precisely, its associated electric field has a dual function. First, it produces the hydrolysis of the water molecules within the liquid meniscus. This process generates the oxyanions that participate in the oxidation process. Second, it drives the oxyanions through the growing oxide. The electric field is introduced by applying a voltage bias either continuously or as a pulse. In the first case, the tip is displaced along the sample while the voltage is switched on. In the second case, the tip rests on a fixed position of the surface during the application of the voltage pulse, then the voltage is switched off and the tip is displaced to another position. In both cases, it is possible to obtain continuous nanostructures. The value of the bias and the oxidation time depend on the material. For silicon surfaces, typical voltage values are in the 5 to 30 V while oxidation times are in the 0.001 to 0.1 s range. The tip and sample surface separation ranges from a few angstroms to 10 nm. The fields reached in o-SPL are extremely high, in the range of  $10^9$  to  $10^{10}$  V/m. Those values explain the capability to pattern a wide range of metallic, semimetallic, semiconductor or organic materials. The use of short oxidation times makes o-SPL also compatible with high-speed AFM operation [53]. The implementation of fast AFM [54] methods could improve the throughput of o-SPL.

### 2.3 Growth kinetics

Low temperature oxidation of solids is a diffusion process where the key factor is to determine whether the oxidation rate is controlled by processes occurring at the metal-oxide interface, by reactions at the oxide-oxygen interface or by diffusion through the oxide. Once the dominant process is established, the activation energy could be determined. In o-SPL, the oxide height exhibits a linear dependence on the applied voltage and a logarithmic dependence on the oxidation time (power-of-time law) [55-57]

$$h(t, V) = Vx[h_0(t/t_0)^\gamma] \quad (1)$$

where  $h$ ,  $V$ ,  $t$  are the total thickness of the oxide, applied voltage and oxidation time;  $h_0$ ,  $t_0$  and  $\gamma$  are fitting parameters;  $\gamma$  depends on the material and pulse oxidation time interval; experimental fittings provide  $\gamma$  values in the 0.1-0.3 range for Si (100) surfaces. Figure 3 shows the dependence of the oxide height and width on the applied voltage and pulse duration. The experiments were performed on a Si (100) surface [57].

The power-of-time law observed experimentally can be deduced by assuming that the rate-controlling step of the oxidation reaction involves the interaction of oxyanions with holes, electrons and defects at a material-oxide interface [58]. To deduce the above equation, requires to consider that the oxide tends to acquire an excess of negative charge whenever the oxide has a greater electron affinity or higher work function than the metal or semiconductor. In fact, Kelvin probe microscopy experiments have shown that o-SPL patterns on silicon surfaces are negatively charged [59, 60]. The production of charged defects leads to a buildup of space charge within the oxide that causes a reduction of the oxidation growth rate for longer voltage pulse times. This leads to the existence of two regimes for the oxide growth as a function of

time [58, 61]. A fast initial oxide growth for short oxidation times (transient regime), say below 0.1 s for silicon surfaces, and a slow growth rate for longer oxidation times (steady-state regime). The transient regime is associated with a direct conversion of material atoms and oxygen ions into oxide. The steady-state regime involves the build-up of space charge defects in the oxide. In this case, the oxidation pathway involves some intermediate stages associated with the space charge build-up [58, 62]. Both regimes could be fitted by a power-of-time law model. In o-SPL most of the patterns are obtained by applying short voltage pulses, say below 0.1 s. Those voltage pulses favor the patterning of nanostructures with optimum aspect ratios [57]. The oxide grows both above and below the silicon baseline. For Si (100) it has been measured that 60% of the oxide thickness is above the silicon baseline (Fig. 3c-d).

To improve further the aspect ratio of the oxide dots, it was proposed to apply an *ac* voltage pulse [63]. The rationale was that the space-charge build up generated during the oxide growth (positive voltages) would be reduced or removed by the application of a negative bias. This in turn would promote the vertical oxide growth over the lateral expansion.

The local anodic oxidation process is accompanied by a Faradic current [64]. Its value depends on the size of the oxide dot. For a 20 nm wide and 3 nm high oxide dot, the current is in the sub-pA range [64, 65].

#### 2.4 AFM operating modes in o-SPL

Oxidation SPL can be performed with the AFM operated in either contact [33, 34, 66] or dynamic mode [35, 37, 45, 57]. In contact AFM (Fig. 4a), the water bridge is formed by the spontaneous condensation of water molecules from the humid air at the tip-sample contact (capillary effect). This process is enhanced by the application of the voltage bias needed to initiate the local anodic oxidation process. In this case, the water bridge is determined by the tip size, the hydrophilic character of the surfaces, the relative humidity and the applied voltage. Those factors make hard to reduce the meniscus size without affecting the overall oxidation process.

When o-SPL is performed by operating an amplitude modulation AFM in the non-contact regime [36-38], the application of an electric field is indispensable to form the water bridge (Fig. 4b). The formation of the water bridge can be followed by recording the cantilever tip deflection before, during and after the application of the pulse (Fig. 4c-4d) [47]. The meniscus size is controlled by the same factors than in contact o-SPL. However, in non-contact o-SPL the water bridge size can be modified by changing the tip-surface separation. It has been shown that, by stretching the water bridge, the lateral size of oxide is reduced [45,47].

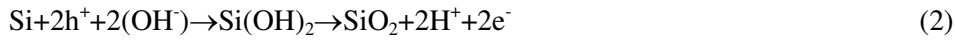
Different types of cantilevers and tips have been used to perform o-SPL experiments. They include doped silicon cantilevers and cantilevers and tips coated with a conductive metallic film [67]. Single wall carbon nanotubes [68] or carbon nanofibers [69] attached at the end of the probe apex of a silicon cantilever have also been used. The flexibility of o-SPL is also reflected by the fact that commercial cantilevers are routinely used for nanolithography. Contact o-SPL experiments are usually performed with Si<sub>3</sub>N<sub>4</sub> cantilevers with a force constant *k* of about 1 N/m. The Si<sub>3</sub>N<sub>4</sub> cantilevers are coated with a conductive film layer made of 5 nm of Cr and 20 nm of Au. The contact AFM feedback is operated by applying a constant force of a few nN. The feedback is switched off during the local oxidation process. To generate a pattern such as a line, the tip is displaced across the sample surface while the voltage is being applied. The tip speed is in the 0.1 to 50 μm/s range while the applied voltage is in the 5 to 30 V range.

Cantilevers for non-contact o-SPL are n<sup>+</sup>-type doped silicon cantilevers with a  $k$  and resonant frequency  $f_0$ , respectively, of about 40 N/m and 350 kHz. The free amplitude is about 5 nm and set-point amplitude ratios are 0.8 to 0.9 (operating amplitude/free amplitude). The patterning is performed by applying a sequence of voltage pulses. Each pulse generates an oxide dot. The pulse duration is in the 0.1 ms to 0.1 s range while the applied voltage is in the 15 to 30 V range. Very small and high aspect ratio oxide dots are generated by combining short voltage pulses (sub-1 ms) and high voltages (above 25 V) [57]. The continuity of a pattern is obtained by displacing laterally the tip between pulses a distance smaller than the dot diameter. The feedback control on the amplitude is switched off during the application of the pulses and activated during the tip displacement between pulses.

For the same relative humidity, voltage bias and oxidation times, the nanostructures generated in non-contact o-SPL have smaller features and higher aspect ratios than those generated contact o-SPL. The tip lifetime and the pattern reproducibility are also increased [70]. This result is a consequence of two effects. First, non-contact o-SPL allows controlling the lateral size of the liquid meniscus since the tip-sample distance could be controlled. This in turn controls the lateral size of the oxide dot. Second, the vertical growth rate is smaller in contact o-SPL. This effect has been attributed to the mechanical energy needed to deflect the cantilever during the growth of the oxide in contact AFM [70]. Contact mode o-SPL offers higher throughputs because the voltage is applied continuously and the microscope feedback is switched off during the whole patterning process.

### 2.5 Oxidation reactions

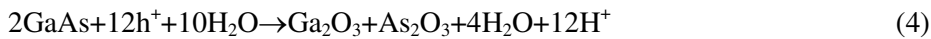
We illustrate three local anodic oxidation reactions involving, respectively, silicon, GaAs and generic metallic surfaces. For silicon, the half-cell reaction on the surface (anode) is



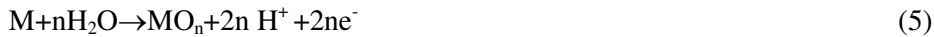
Charge and mass conservation requires another half-cell reaction at the tip (cathode), in this case, hydrogen generation



For GaAs, the half-cell electrochemical reaction happening on the surface is



In general, for a metallic surface the half-cell reaction (anode) can be described as



Different spectroscopy analysis of o-SPL patterns generated on Si and GaAs have confirmed the formation of, respectively, silicon and gallium arsenide oxides [44, 71, 72].

### 2.6 The instrument

A variety of instruments and cantilevers have been applied to perform oxidation SPL. In fact, any AFM could be adapted for oxidation SPL (Fig. 5). The nanolithography application just requires some minor modifications such as the incorporation of additional circuits to apply voltage pulses and a software to control the tip motion while patterning.

In o-SPL, the AFM head should be placed in a closed box with inlets for dry and H<sub>2</sub>O saturated nitrogen to control the relative humidity with accuracy. The relative humidity should be kept in the 30% to 60% range. This range facilitates the formation of a water bridge. In some instruments, the use of higher values in combination with the high voltages applied to the *xy* scanner could damage the scanners.

### **3. Advanced nanopatterning, template growth and device fabrication.**

The direct result of an o-SPL experiment is to generate a very thin and localized oxide. The o-SPL oxides have three main functionalities: templates, masks and dielectric barriers. In the following sections we will illustrate the role of the above functionalities for nanopatterning and device fabrication.

#### *3.1 Nanopatterning*

Oxidation scanning probe lithography allows the direct (resist-less) modification of small areas to create patterns with a specific functionality. Silicon, gallium arsenide compounds, tantalum and titanium surfaces were the first materials patterned by o-SPL. Since then, the type and chemical nature of the materials patterned or modified by o-SPL has considerably grown. It includes metals such as Ni [73] or Hf [74] to semiconductors such as SiC [75], to dielectrics such as Si<sub>3</sub>N<sub>4</sub> [76], to complex oxides such as LaBaMnO [77] and two-dimensional layered materials such as graphene [27], MoS<sub>2</sub> [78, 79], WSe<sub>2</sub> [80] and other transition metal dichalcogenides [81]. Several self-assembled monolayers and polymers have also been patterned by o-SPL (see below).

Figure 6 illustrates some of the nanopatterning capabilities of o-SPL. Silicon oxide line arrays with a periodicity of 15 nm (7.5 nm half pitch) have been patterned on Si(100) surfaces (Fig. 6a). The fine tuning of the voltage and the oxidation time during the lithography enables the generation of grey-scale patterns on silicon surfaces with remarkable contrast [82] (Fig. 6b). The capability to pattern novel materials is shown by the array of 13 nm dots patterned on a WSe<sub>2</sub> flake [80] (Fig. 6c). Ferritin proteins have been precisely positioned on top the o-SPL patterns by modulating the electrostatic interaction between the patterns and the proteins [83] (Fig. 6d). The ferritin pattern was generated by arranging chains of single ferritin proteins in parallel arrays. This example illustrates the combination of top-down and bottom-up lithography methods. The control on the feature size provided by o-SPL is also illustrated by the patterning a 10 nm constriction on a graphene flake [84] (Fig. 6e) or by the fabrication of sub-50 nm metallic islands on TaS<sub>2</sub> thin films [85] (Fig. 6f).

Other examples to tailor functional surfaces at the nanoscale are illustrated by the change in the work function of silver nanoparticle sheets to tune the plasmonic properties [86], the tunability of the surface adhesion by patterning different geometric shape arrays on a GaAs substrate [87] or the fabrication of GaO<sub>x</sub> nanotips on the surface of a GaN-based light emitting diode to improve the light extraction efficiency [88].

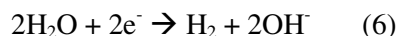
The above results, in particular Figure 6b and 6c, illustrate the degree pattern reproducibility achieved by o-SPL, respectively, in the sub-50 and sub-20 ranges. Pattern reproducibility in the sub-10 nm domain (Fig. 6a, 6d and 6e) is highly dependent on preserving the tip shape and the size and geometry of the water bridge.

### 3.2 Template growth and molecular architectures

The positioning and/or assembly of very small objects in preferential sites or in a preferential configuration to make them an active part of a functional system are an attractive feature of o-SPL. Some examples are provided by template growth of organic semiconductors [89]; the nanoscale organization of molecule-based magnetic compounds [90, 91], biomolecules [83, 92, 93], functional dyes [94] or the guided assembly of block-copolymers [95].

Oxidation SPL has been extensively applied to modify self-assembled monolayers [83, 96-109]. Those experiments have produced remarkable examples on the guided assembly of metallic nanoparticles on top of self-assembled monolayers [100-103]. In particular, Sagiv's group has pioneered the oxidation of the terminal groups of self-assembled monolayers to build molecular architectures [100, 104, 105]. In one approach, o-SPL was used to locally oxidize an OTS (n-octadecyltrichlorosilane,  $\text{CH}_3\text{-(CH}_2\text{)}_{17}\text{-SiCl}_3$ ) monolayer on a Si substrate. The process transforms the methyl ( $\text{CH}_3$ ) terminated groups into carboxylic acid ( $\text{COOH}$ ) groups. In a second step a bilayer is formed in the modified region. An additional chemical process generates amino-terminated templates in the modified regions. These templates guide the surface assembly and site specific anchoring of gold nanoparticles from a colloidal solution [100, 105].

A scheme of the oxidation process of the OTS layer is shown in figures 7a-7e. In the local oxidation of methyl terminated chains, the following chemical reactions take place at the tip



And at the sample surface,



The carboxyl ( $\text{COOH}$ ) terminated groups are chemically active. They have been used as templates to attach metallic nanoparticles [104], to place a silver nanoparticle between a metallic gap [106] or to assemble two individual carbon nanotubes in a cross configuration [107].

The strength of the applied voltage and its duration control the material modified by the tip. For small and short voltage pulses ( $<8$  V,  $\sim 1$  ms) the oxidation is confined to the functionalized organic monolayer. However, for higher and longer voltage pulses the initial monolayer is totally degraded and the oxidation of the underlying Si substrate occurs [108]. By changing the o-SPL parameters, ring-like structures that have a core made of silicon oxide and a rim made of the SAM molecules have been fabricated [109].

Oxidation SPL has been applied to position quantum dots on predefined sites of a semiconductor surface. In one approach, an array of nano-oxides was patterned on a GaAs (001) sample, then the nano-oxides were selectively etched leaving an array of holes. Those holes were used as preferential sites for the nucleation of InAs quantum dots [110, 111]. In another application, an array of nanoholes were formed on a silicon surface by the combination of local oxidation and dry etching. Those holes were used as traps to pin colloidal PbS quantum dots [112].



Oxidation SPL has been applied to guide the direct self-assembly of block copolymers (BCPs) [95]. Block copolymers are macromolecules that are formed by, at least two chemically distinct polymer chains (blocks) joined by inter-block covalent bonds. An attractive feature of these materials for lithography is the capability to form dense periodic nanoscale patterns over large areas, what means potentially a high throughput [113]. Guiding patterns were defined by o-SPL on a polymer brush layer of hydroxyl-terminated polystyrene (PS-OH) deposited on a silicon surface (Fig. 7f). The block copolymer used in the experiment consists in poly (styrene-*b*-methacrylate) (PS-*b*-PMMA 50:50,  $M_n = 35 \text{ kg}\cdot\text{mol}^{-1}$ , PDI = 1.12). After o-SPL, the block copolymer is spin-coated onto the brush layer. Then, the sample is annealed to self-assemble the block copolymer (Fig. 7g). Finally, the PMMA domains are removed by oxygen plasma (Fig. 7h). The aligned block copolymers have denser periodicities than the width of the guiding patterns that confine them, presenting density multiplication factors between 3 and 7, with BCPs with 14 nm half-pitch for the last factor. Figure 7h shows the difference in periodicity between the guiding patterns and the ordered BCPs.

### 3.3 Dielectric barriers and masks

On some materials such as GaAs, Ti or Nb the local oxides have good insulating properties to act as a dielectric barrier to separate two electron conducting regions in a device. This has led to the direct fabrication of several devices such as quantum point contacts, single electron transistors or metal-oxide field-effect transistors [71, 114, 115]. In fact, the first transistor with a features claimed to be in the sub-10 nm range was reported by o-SPL [116].

On other materials such as silicon, aluminium, graphene or MoS<sub>2</sub>, the local oxides could be used as etching masks during pattern transfer processing. For example, it has been demonstrated that ultrathin silicon oxide masks (0.3-1 nm) are very efficient in reactive ion etching processes to transfer the pattern onto a 12 nm thick silicon active layer of an ultrathin silicon on insulator substrate. An etching selectivity of 11 has been reported [117]. Silicon oxide masks have been used to fabricate a variety of silicon devices [76, 118-121]. Local anodic oxidation of aluminum has produced a highly selective dry etching mask on CMOS processed chips. Those masks have been applied to fabricate nanomechanical resonators [122]. Spintronic devices on magnetite have been designed by using o-SPL to fabricate Mo and poly-methyl methacrylate nanomasks [123].

### 3.4 Minimum feature size

In table I we summarize the main achievements of o-SPL in terms of feature size. We include contributions that report feature sizes below 15 nm. Feature sizes in the sub-10 nm range have been reported on Si [121], Ti [124] and graphene surfaces [125]. Most publications report the feature size data in terms of the full width at half maximum (FWHM). This is a common procedure to report AFM width measurements. This approximation compensates for the dilation effect introduced by the finite size of the tip.

To prepare the table, we have considered experimental results that fully support the reported feature size. In some publications, the claims in terms of minimum feature sizes have not been supported by high resolution images or cross-section profiles.

#### 4 Nanoscale electronic devices

Oxidation SPL has been applied to fabricate silicon nanowire field-effect transistors from a silicon on insulator substrate [120, 121, 127]. We describe the main steps of the fabrication process. First, two metal electrodes are defined as localization markers on the top silicon layer by photolithography (Fig. 8a). Then, o-SPL is performed to define an oxide line between the markers (Fig. 8b). The AFM tip should not contact the metallic electrodes. Otherwise, the high electric fields applied could modify the electrodes. Another photolithography step is performed to contact the nanowire with the metal electrodes, source and drain (Fig. 8c). The oxide pattern is transferred to the silicon by using reactive ion etching. This process removes the silicon surface unprotected by the oxide mask (Fig. 8d). The fabrication process leads to a back-gate Si nanowire field-effect transistor (FET). A rapid thermal annealing treatment is commonly applied to improve the electric properties of the metal-semiconductor contact [127]. These transistors have been employed as label-free biosensors to track the process of DNA repair by the RecA protein [128]. To fabricate the Si nanowire FET biosensor, the device is covered by a microfluidic channel that protects the metallic electrodes and exposes the transistor channel to the solutions. Figure 8e shows the changes in the nanowire resistance as a function of the analyte solution surrounding the nanowire. A minimum is observed when the RecA protein is interacting with the ssDNA. The inset on the left shows an optical image of the device and the image on the right shows the nanowire bridging the gold electrodes.

Oxidation SPL has been used to fabricate nanoscale field-effect transistors on thin-layer transition metal dichalcogenides [78, 80]. In this application, o-SPL is used to define the channel length of the device by separating different conductive regions with dielectric barriers. First, a thin flake of the material is deposited or grown on an insulator substrate such as a  $\text{SiO}_2$  or  $\text{HfO}_2$ . Then, the source and drain contacts are fabricated by photolithography or electron beam lithography. Then, o-SPL is performed to define oxide lines that constitute the boundaries of the nanochannel. The oxidation has to penetrate through the whole thickness of the flake to ensure the isolation of the nanochannel from the rest of the transition metal dichalcogenide surface. Figure 9a shows, an AFM image of a  $\text{MoS}_2$  thin layer nanoFET [78].

The direct and resist-less fabrication of dielectric barriers offered by o-SPL has led to its use to generate a large number of graphene-based nanoelectronic devices [27, 129-133]. Figure 9b (top panel) shows the AFM topographic image of a quantum point contact where the source, drain, channel and side gates have been defined by separating the areas with o-SPL made insulating barriers and plasma etching [130]. The conductance as a function of the applied source-drain (vertical axis) and gate (horizontal) voltages of the device is presented in figure 9b (bottom panel).

Metal ion transport ( $\text{Ag}^+$ ,  $\text{Ti}^{4+}$ ) in the absence of a solvent have been achieved by a device fabricated with o-SPL [134]. Figure 9c illustrates the flux of silver ions in dry conditions. The process to fabricate this device consists in the local oxidation of a monolayer of n-octadecyltrichlorosilane ( $\text{SiCl}_3 - (\text{CH}_2)_{17} - \text{CH}_3$ ) molecules into  $-\text{COOH}$  terminated confined paths. Two silver electrodes, the anode and cathode, are placed between the boundaries of the  $-\text{CH}_3$  and  $-\text{COOH}$  terminated surfaces by electron-beam evaporation. Under the application of a bias between the electrodes, the silver ions move towards the cathode by displacing the protons from the carboxyl terminated groups until all these sites have been released their protons and filled by the metal cations.

The direct approach to define ultra narrow dielectric barriers on selected regions of a surface has been exploited to fabricate sophisticated quantum devices on semiconductor heterostructures [71, 114, 135-139] such as quantum point contacts, quantum dots, double quantum dots and quantum rings [71]. A two-dimensional electron gas (2DEG) can be generated near the outer surface of a GaAs-AlGaAs heterostructure [71] (Fig. 10a). After o-SPL on the GaAs top surface, the regions of the 2DEG below the oxide line are depleted creating selective areas with higher resistance on the 2DEG channel (Fig. 10b). To achieve the depletion of the 2DEG by o-SPL, the electron gas layer should not be more than 50 nm below the surface. Typical o-SPL parameters for the fabrication of this type of nanostructures are a relative humidity, range of voltage and writing speed of, respectively, 38%, 10-25V and 0.2  $\mu\text{m/s}$ . A *p*-type GaAs quantum point contact as shown in figure 10c [135]. The depleted 2DEG regions define and separate the quantum point channel from the different gates used to modulate the transport through the channel. For some applications, the in-plane gates do not offer enough electrostatic control or do not allow the individual tuning of the different parts of a multicomponent device, so additional top gates are required. In this case, a second layer of a Ti thin film is deposited (Fig. 10d) on the top GaAs layer. The Ti oxides defined by o-SPL act as dielectric barriers that separate the different top gate segments (Fig. 10e). The applied voltage to oxidize the Ti is smaller than the one used to oxidize the GaAs to avoid further modifications of the GaAs layer below. Figure 10f shows a quantum dot connected to four leads via four quantum point contacts (labelled A, B, C, D) [114]. The in-plane gates defined in the first layer step are represented by pg1 and pg2 and the Ti top gates defined in the second layer step are labelled as tg1, tg2 and tg3.

The above examples have been chosen to illustrate the capabilities, achievements and potential of o-SPL to fabricate nanoelectronic devices. Other applications of o-SPL are the fabrication of single photon detectors [140], ultraviolet sensors [141], photonic nanocavities [142], ferromagnetic tunnel junction devices [126], resistive random access memories [143], spintronic devices [144], nano-memristors [145], magnetic nanoparticles embedded in oxide for data storage [146] and superconducting structures [147]. Oxidation SPL has been used to generate site-controlled arrays of InAs/GaAs quantum dots [110, 111]. The quantum dots have shown a satisfactory optical response as measured by microphotoluminescence and photon correlation experiments [148].

## 5. Beyond local anodic oxidation

We have mentioned the similarities between an o-SPL interface and an electrochemical cell. The sign of the voltage determines which electro-chemical reaction will take place on the sample surface. In o-SPL the sample is biased positively with respect to the tip which leads to the oxidation of the sample surface. However, in some materials the reduction reaction could be achieved by reversing the voltage polarity. Thus, the same SPL set up has been used for either the oxidation (sample positive) and reduction (sample negative) on the same area of graphene surface [149]. In the same manner, the nature of the gas surrounding the interface will determine the composition of the nanopatterns. Silicon oxide and carbonaceous structures have been generated by using as the media an organic solvent, 1,3,5-trimethylbenzene under ambient conditions [150]. The application of a negative voltage to the tip with respect to the silicon surface yields the formation of silicon nanostructures, while the application of a positive tip bias produces the decomposition of the precursor molecule in the vicinity of the tip and the

consequent deposition of carbonaceous nanostructures on the surface. The replacement of the water by ethanol or octane vapours has led to the fabrication of carbonaceous nanostructures without reversing the bias polarity [44, 151]. The role of the water bridge as the supplier of the oxyanions could be replaced by using an enriched ozone environment [78, 152] or by using a suitable polymer layer [153]. In some cases, the o-SPL set up has been used to study chemical reactions unrelated to patterning applications such as the decomposition of carbon dioxide molecules in the presence of high electric fields [40, 154]

## **6. Parallel patterning**

The sequential character of o-SPL makes the patterning process relatively slow. This factor together with a maximum  $xy$  scanning range of  $10^4 \mu\text{m}^2$  limit the effective patterning area in o-SPL to  $400 \mu\text{m}^2$ . The above features make o-SPL slow for technological-oriented applications. Several approaches are being explored to overcome the above limitation. The incorporation of high speed AFM methods [53] in o-SPL could improve the patterning speed and the patterning area. Large regions ( $1 \text{ cm}^2$ ) have been patterned by using an array of 50 cantilevers [155]. Other alternatives to up-scale the local oxidation process include the use of a conductive stamp with multiple protrusions as the cathode electrode [156-157]. Then, in a single step a large area could be patterned with millions of nanostructures. This approach has been applied to pattern silicon surfaces with oxide patterns [158-159], to modify pentacene layers [160] or to build molecular architectures [161]. Nanostructures of different chemical compositions have been generated by either changing the polarity between the stamp and the sample or the gas environment, [40,162].

## **7. Summary**

Oxidation SPL has experienced a steady evolution since the serendipitous discovery of the local oxidation of a silicon surface. Since then, the physical and chemical processes governing the patterning in o-SPL have been thoroughly studied. Those studies have underlined the roles of the water meniscus and the voltage bias to control the pattern size.

The general character of the local anodic oxidation process, its robustness and resist-less features have enabled the patterning of a wide range of materials from metals to semiconductors; from self-assembled monolayers to polymers; from single biomolecules to organic macromolecules.

Practically any AFM can be transformed into an instrument to perform o-SPL experiments without compromising the intrinsic metrology and positioning capabilities of the AFM. Those factors and the satisfactory performance of the nanostructures and/or devices have contributed to the quiet and widespread use of o-SPL.

Oxidation SPL is a sequential lithography. This makes the patterning process intrinsically slow for technological-oriented applications. This fact might prevent its incorporation into large-scale manufacturing of materials. However, this limitation will not affect its evolution and applications in basic and applied research where the readiness of o-SPL to pattern new materials and fabricate advanced devices will always be valued and exploited.

## **Acknowledgement**

This work was funded by the European Union FP7/2007-2013 under Grant Agreement No. 318804 (SNM) and the Ministerio de Economía y Competitividad (Spain) under grants MAT2013-44858-R, MAT2015-69725-REDT and MAT2016-76507-R.

## Figures and figure captions

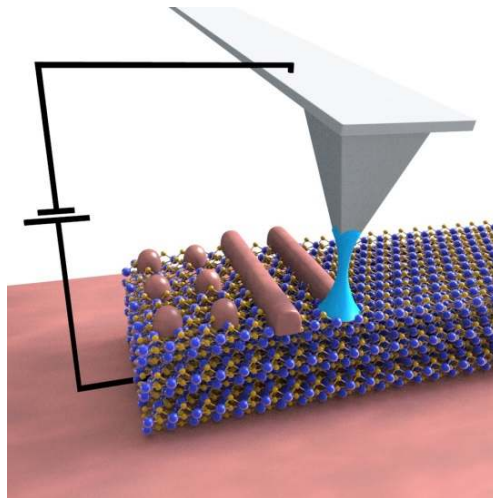


**Figure 1.** General scheme of nanopatterning in o-SPL.

(a)		STM	dynamic AFM	high speed AFM
1990	1993	1994-1998	1993-1999	1998-2004
contact AFM		meniscus	kinetics	2009
(b)		Si, Ta, Nb, Ti, GaAs	graphene	transition metal dichalcogenides
1990-1998	1995-2005	2008-2011	2003-2010	2015-2016
SAM		Protein, macromolecules patterning	Grey-scale patterning	2016
(c)		Metal-oxide transistors	Quantum devices (III-V compounds)	graphene devices
1995-1998	1997-2008	1998-2002	2002-2011	2008-2013
1997-2008	1998-2002	2002-2011	2007-2012	2015-2016
Single electron transistors		Si nanowire devices	optical devices	TMD devices

**Figure 2.** Milestones in the evolution of oxidation SPL. (a) Relevant developments in instrumentation and mechanism. (b) Materials. (c) Devices. The years indicate either the beginning of the activity or the period where the fundamental understanding was developed. In many applications an intense and rich activity is ongoing.

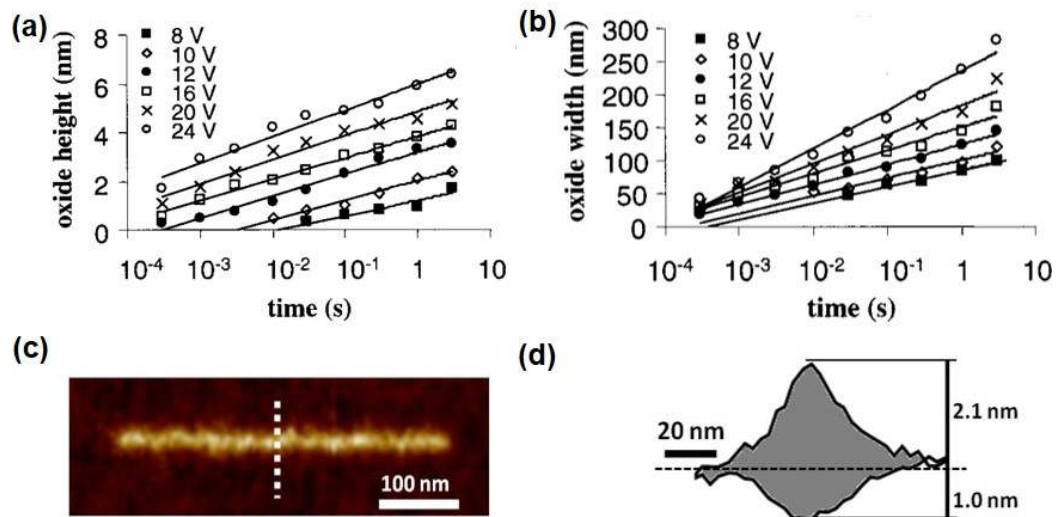


**Figure 3.** Kinetics of silicon oxide growth in o-SPL. (a) Oxide height measured from the silicon baseline as a function of the oxidation time and applied voltage. (b) Oxide width as a function of the oxidation time and applied voltage. (c) AFM image of a silicon oxide line. (d) The cross-section along the marked line (bottom image) shows both the oxide above and below the silicon surface baseline (dash line). Data in (a) and (b) adapted from [57]. Data in (c) and (d) adapted from [117].

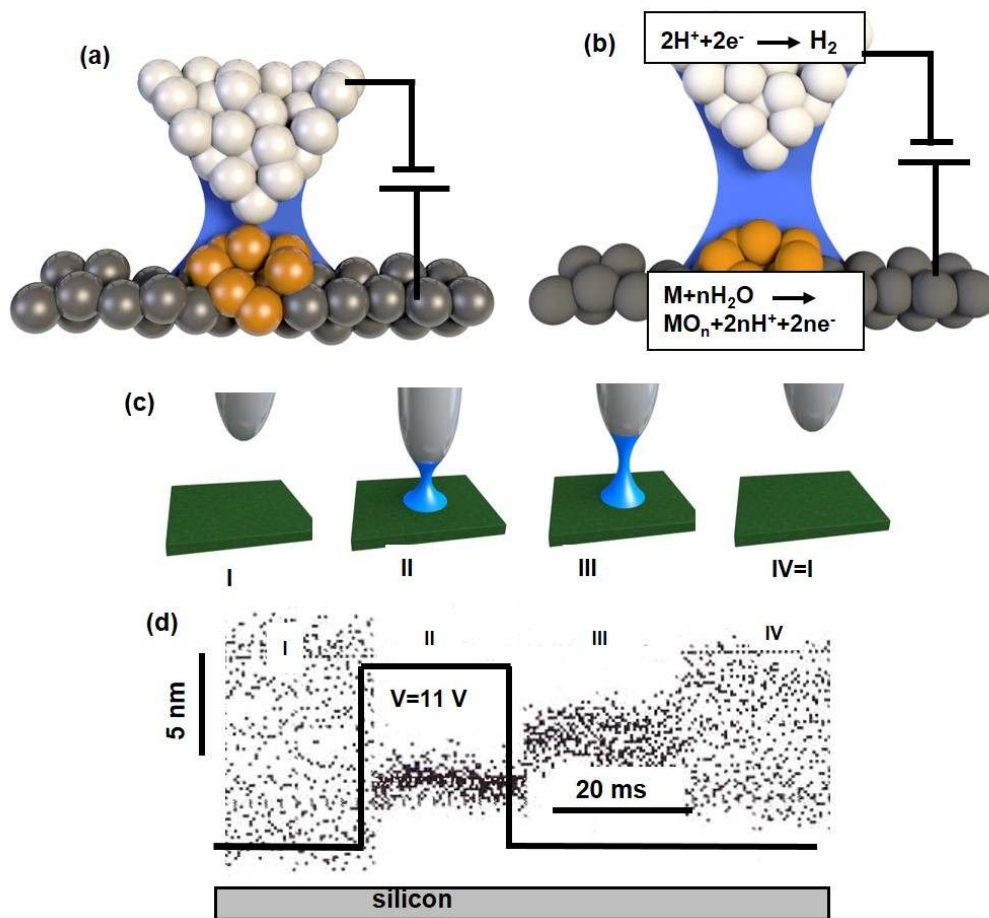


**Figure 4.** Scheme of the tip-sample interface in o-SPL. (a) Contact. (b) Non-contact. (c) Main steps in the formation of a water bridge in non-contact o-SPL. In step I the tip oscillates above the surface. Each point in the graph indicates the position of the tip with respect to the sample surface. In step II the electric field induces the formation of the bridge. The electrostatic and the capillary forces draw the tip closer to the sample surface. In step III the voltage is switched off and the tip (average position) is slightly retracted from the sample. The capillary force keeps the amplitude at a value smaller than in step I. Finally, the tip retracted by the  $z$ -piezo scanner until the amplitude recovers its initial value (IV). (d) Tip instantaneous position with respect to the sample surface in a non-contact o-SPL experiment. Each dot in the graph represents the instantaneous tip deflection. Data adapted from [45, 47].



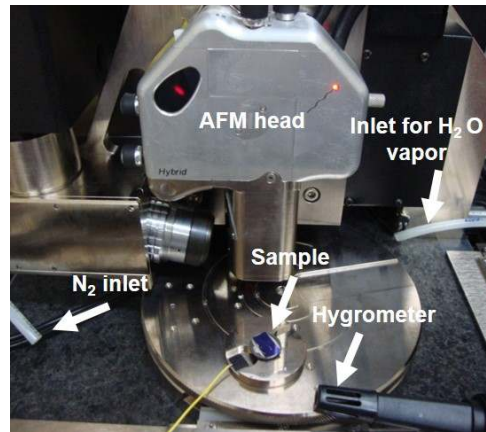


**Figure 5.** Photograph of an AFM adapted for o-SPL. The AFM head, xyz scanner and sample based are enclosed in a chamber (not shown) with inlets for controlling the water vapor pressure and monitoring the relative humidity and temperature.

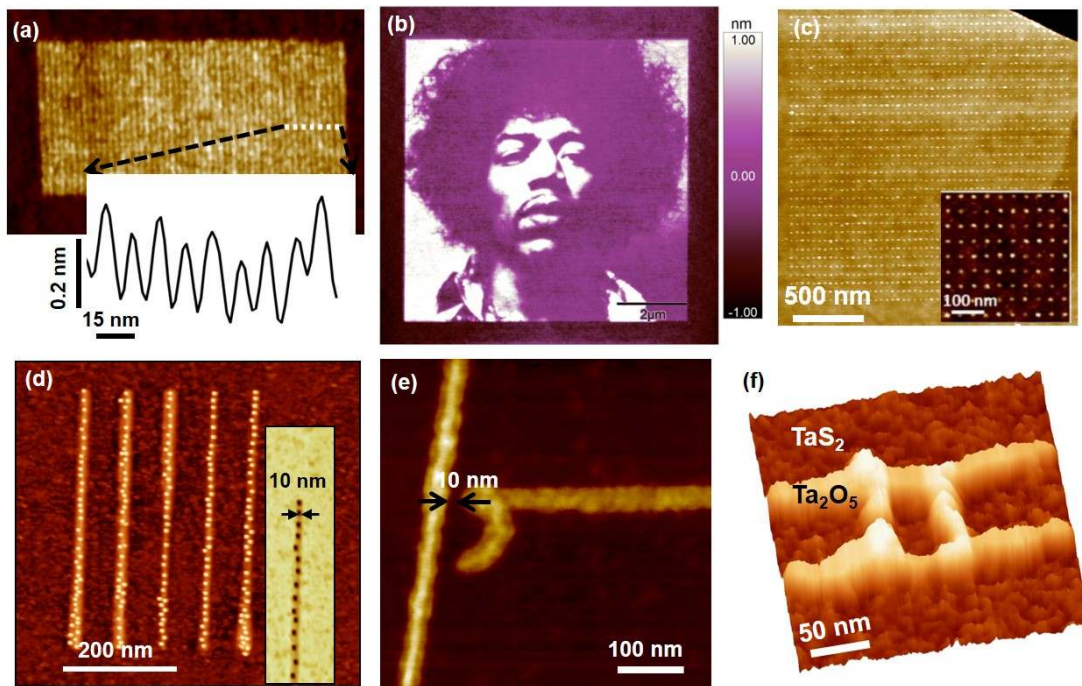


**Figure 6.** AFM images of nanopatterns generated by o-SPL. (a) Array of silicon oxide lines with a periodicity of 15 nm. (b) Greyscale patterning of a photograph of Jimmy Hendrix with sub-1 nm depth precision written on a silicon surface. (c) AFM image of an array of dots patterned by o-SPL on a few layer WSe<sub>2</sub> flake. The dots are 13 nm in width, 1 nm in height and are separated by 40 nm. The inset shown in a smaller region of the pattern. (d) Array of ferritin proteins. The inset shows (AFM phase image) the presence of a 12 nm wide line that contains a chain of ferritin molecules. (e) Nano-oxide lines on graphene grown on SiC. The oxide lines define a quantum dot connected with the graphene surface by 10 nm and 22 nm wide constrictions. (f) Sub-50 nm metallic island on TaS<sub>2</sub> thin film. Data in (c) and (d) adapted, respectively, from [80] and [83]. Data in (b) reported with permission from [82]. Data in (f) reported with permission from [85].

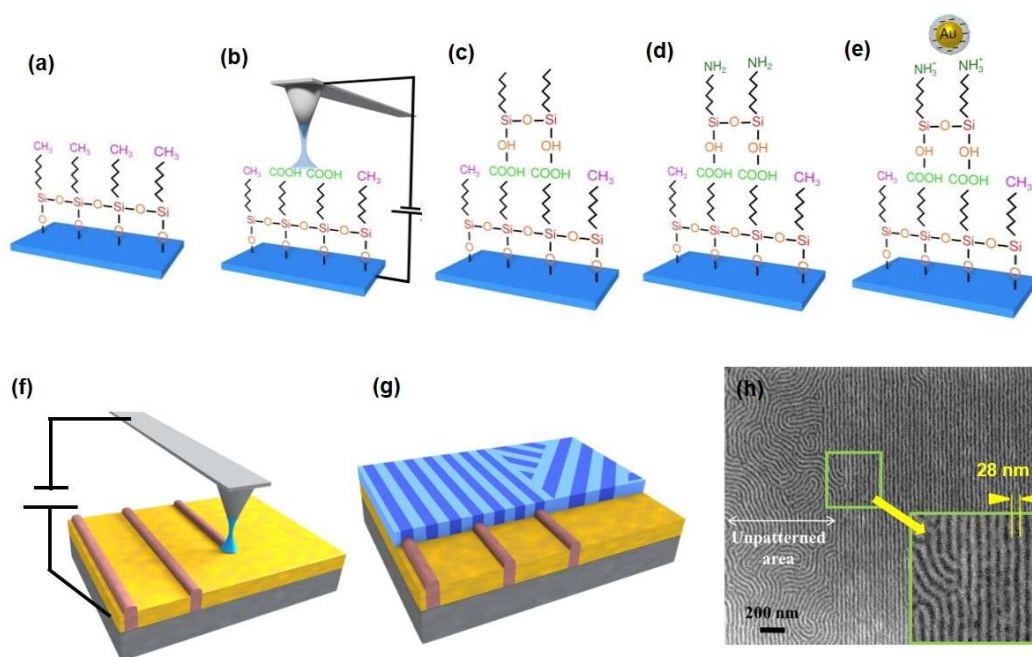


**Figure 7.** (a) Fabrication of molecular architectures by combining o-SPL and self-assembled monolayers. Functionalization of a silicon surface with a self-assemble monolayer. (b) Selective oxidation of the terminal groups. (c) Self-assembled of a different layer. (d) Amino functionalization of the 2<sup>nd</sup> layer. (e) Attachment of gold nanoparticles from a colloidal solution (f) Guided self-assembly of block copolymers by o-SPL. Oxidation SPL defines some patterns on a polymer brush. (g) The interaction of the patterns with a block copolymer promotes the organization of parallel structures. (h) The SEM image illustrates the different structure of the copolymer inside and outside the patterned region. Data in (h) reported with permission from [95].

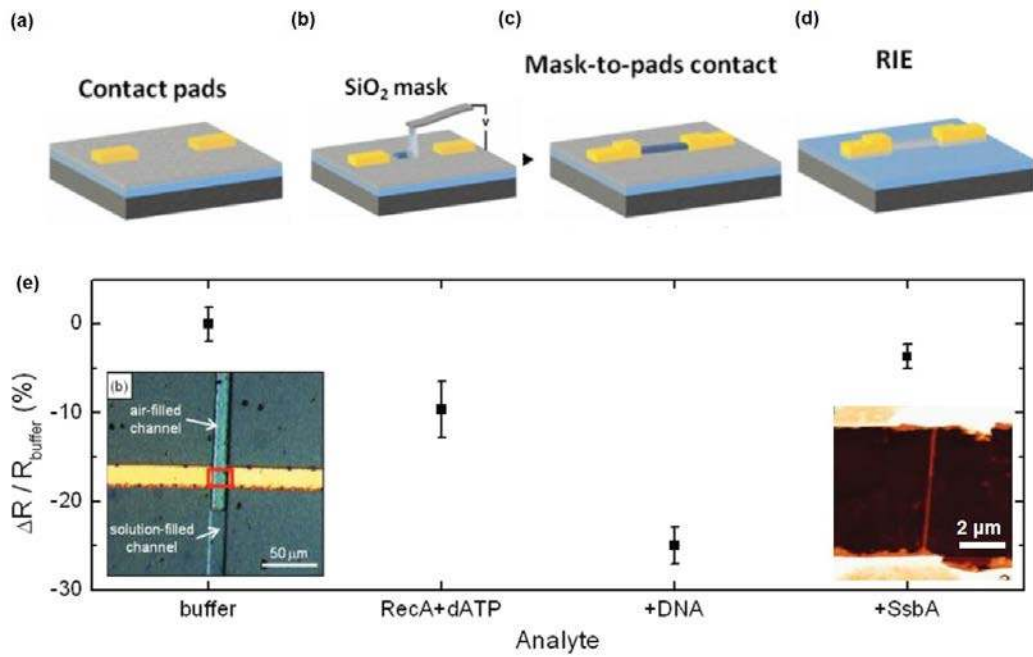


**Figure 8.** (a)-(d) Main steps in the fabrication of a Si nanowire field-effect transistor by o-SPL. (a) Metal pads defined by photolithography to be used as markers for the fabrication of the oxide masks. (b) Oxide masks for the fabrication of a Si nanowire. (c) Second photolithography step to connect the first metal pads with the nanowire to define the source and drain contacts. (d) After reactive ion etching processing, the silicon layer unprotected by the oxide mask is removed. The final result is a back gated Si nanowire FET. (e) Change on the resistance of a Si nanowire FET biosensor as a function of the different analytes. The left inset represents an optical image of the microfluidic channel that directs the chemical analytes to the nanowire. The right inset shows a topographic AFM image of the nanowire channel between the source and drain electrodes. Data in (a)-(d) adapted from [127]. Data in (e) adapted from [128].

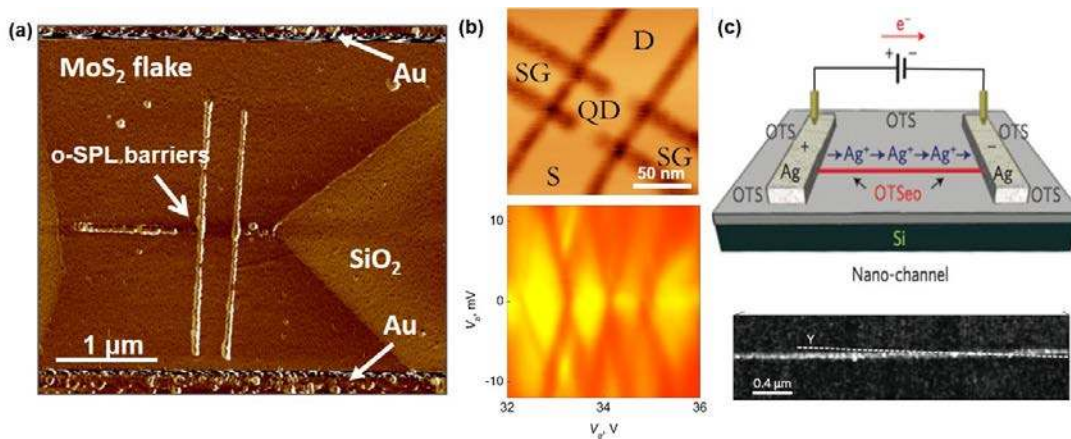


**Figure 9.** Some devices fabricated by o-SPL. (a) AFM phase image of a nanoscale MoS<sub>2</sub> monolayer FET. A 200 nm wide channel is defined by the fabrication of insulating barriers on MoS<sub>2</sub> by o-SPL. (b) The top panel is an AFM friction image of the quantum dot device created by o-SPL on graphene. The bottom panel shows the Coulomb diamond structures of the quantum dots as a function of the gate and source-drain voltages, horizontal and vertical axis respectively. (c) The top panel represents a scheme of the ion transport device and the flux of the silver ions through the channel when a bias is applied. The bottom panel is an AFM image

of a section of the channel after the bias was applied for a few seconds Data in (a) adapted from [78]. Data in (b) and (c) reproduced with permission, respectively, from references [130] and [134].

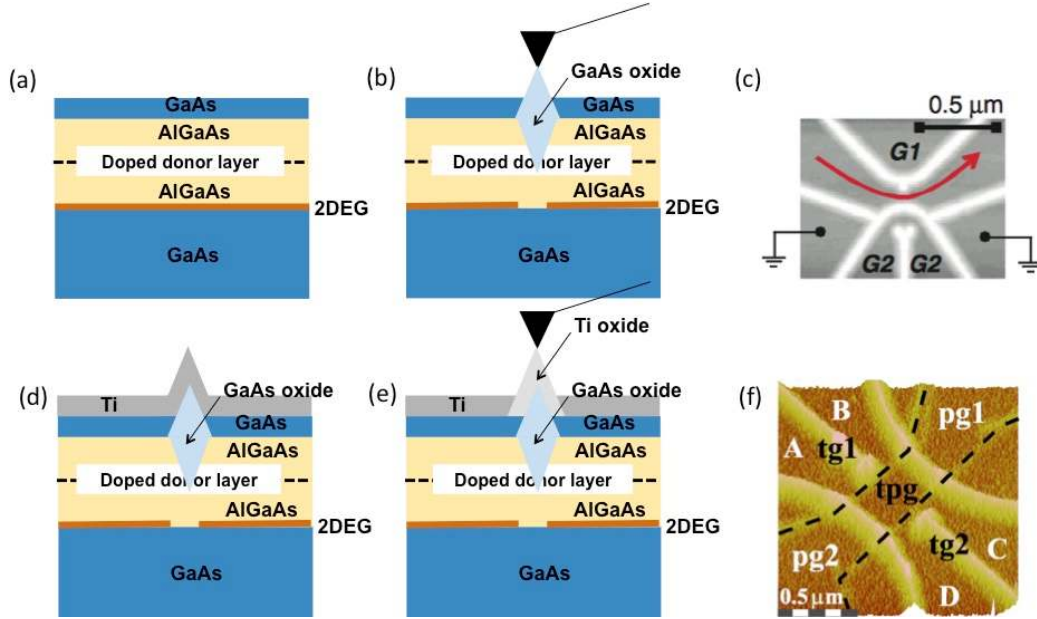


**Figure 10.** Quantum transport devices fabricated by o-SPL on semiconductor heterostructures. (a) Scheme of the heterostructure. (b) Application of o-SPL to deplete the 2DEG layer underneath the local oxides. This creates an effective dielectric barrier that defines the different components of the device. (c) AFM topographic image of a quantum point contact fabricated by following the process explained in (a) and (b). (d) Scheme of the deposition of a thin Ti layer after (b). (e) Another o-SPL step to oxidize selected areas of Ti to define additional gates for quantum devices. (f) AFM image of a quantum dot fabricated according to the process explained in (a), (b), (d), (e). Data in (c) and (f) reproduced with permission, respectively, from references, [135] and [114].

Material	Feature size (FWHM) (nm)
<sup>121</sup> Si nanowire	8 (4 nm after tip deconvolution)
<sup>124</sup> Ti	8
<sup>126</sup> Nb	10
<sup>125</sup> Graphene	10
<sup>80</sup> WSe <sub>2</sub> thin layer	12
<sup>95</sup> Block copolymer PS-b-PMMA	14 nm (half-pitch)

**Table 1.** Sub-15 nm nanostructures fabricated by o-SPL

## References

- [1] Binnig G and Rohrer H 1999 In touch with atoms *Rev. Mod. Phys.* **71** S324-30
- [2] Eigler D M and Schweizer E K 1990 Positioning single atoms with a scanning tunneling microscope *Nature* **344** 524-6.
- [3] Lyo I W and Avouris P 1991 Field-induced nanometer to atomic-scale manipulation of silicon surfaces with the STM *Science* **253** 173-6
- [4] Dagata J A, Schneir J, Harary H H, Evans C J, Postek M T, and Bennet J 1990 Modification of hydrogen-passivated silicon by a scanning tunneling microscope operating in air *Appl. Phys. Lett.* **56** 2001-3
- [5] Mamin H and Rugar D 1992 Thermomechanical writing with an atomic force microscope tip. *Appl. Phys. Lett.* **61** 1003-5
- [6] Vettiger P, Despont M, Drechsler U, Durig U, Haberle W, Lutwyche M I, Rothuizen H, Stutz R, Widmer R and Binnig G K 2000 The “Millipede” – more than thousand tips for future AFM storage *IBM J. Res. Dev.* **44** 323-40
- [7] Szoszkiewicz R, Okada T J, Simon C, Li T D, King W P, Marder S R and Riedo E 2007 High-speed, sub-15 nm feature size thermochemical nanolithography *Nano Lett.* **7** 1064-9
- [8] Carroll K *et al* 2014 Parallelization of thermochemical nanolithography *Nanoscale* **6** 1299-1304
- [9] Pires D, Hedrick J L, Silva A D, Frommer J, Gotsmann B, Wolf H, Despont M, Duerig U and Knoll A W 2010 Nanoscale Three-dimensional patterning of molecular resists by scanning probes *Science* **328** 732-5
- [10] Holzner F, Kuemin C, Paul P, Hedrick J L, Wolf H, Spencer N D, Duerig U and Knoll A W 2011 Directed placement of gold nanorods using a removable for guided assembly *Nano Lett.* **11** 3957-62
- [11] Rawlings C, Wolf H, Hedrick J L, Coady D J, Duerig U and Knoll A W 2015 Accurate location and manipulation of nanoscaled objects buried under spin-coated films *ACS Nano* **9** 6188-95.
- [12] Garcia R G 1992 Atomic-scale manipulation in air with the scanning tunneling microscope *Appl. Phys. Lett.* **60** 1960-2
- [13] Vasko S E, Kapetanovic A, Talla V, Brasino M D, Zhui Z, Scholl A, Torrey J D and Rolandi M 2011 Serial and parallel Si, Ge, and SiGe direct-write with scanning probes and conducting stamps *Nano Lett.* **11** 2386-9
- [14] Kaestner M and Rangelow I W 2012 Scanning probe nanolithography on calixarene *Microelectron. Eng.* **97** 96-9
- [15] Salaita K, Wang Y and Mirkin C A 2007 Applications of dip-pen nanolithography *Nature Nanotechnol.* **2** 145-55

- [16] Cavallini M, Biscarini F, Leon S, Zerbetto F, Bottari G and Leigh D A 2003 Information storage using supramolecular surface patterns *Science* **299** 531-3
- [17] Tseng A A 2011 Removing material using atomic force microscopy with single- and multiple-tip sources *Small* **7** 3409-27
- [18] Felts J R, Onses M S, Rogers J A and King W P 2014 Nanometer scale alignment of block-polymer domains by means of a scanning probe tip *Adv. Mater.* **26** 2999-3002
- [19] Garcia R, Martinez R V and Martinez J 2006 Nanochemistry and scanning probe nanolithographies *Chem. Soc. Rev.* **35** 29-38
- [20] Obermair C, Kress M, Wagner A and Schimmel T 2012 Reversible mechano-electrochemical writing of metallic nanostructures with the tip of an atomic force microscope *Beilstein J. Nanotech.* **3** 824-30
- [21] Liu H, Hoepfner S and Schubert U S 2016 Nanoscale materials patterning by local electrochemical lithography *Adv. Eng. Mater.* **18** 890-902
- [22] Liu H, Hoepfner S and Schubert U S 2016 Reversible nanopatterning on polypyrrole films by atomic force microscope electrochemical lithography *Adv. Funct. Mater.* **26** 614-9
- [23] Arruda T M, Kumar A, Jesse S, Veith G M, Tselev A, Baddorf A P, Balke N and Kalinin S V 2013 Toward quantitative electrochemical measurements on the nanoscale by scanning probe microscopy: Environmental and current spreading effects *ACS Nano* **7** 8175-82
- [24] Zhang K, Qiang F, Pan N, Yu X, Liu J, Luo Y, Wang X, Yang J and Hou J 2012 Direct writing of electronic devices on graphene by catalytic scanning probe lithography *Nat. Commun.* **3**:1194
- [25] Carnally S A M and Wong L S 2014 Harnessing catalysis to enhance scanning probe nanolithography *Nanoscale* **6** 4998-5007
- [26] Fuechsle M, Miwa J A, Mahapatra S, Ryu H, Lee S, Warschkow O, Hollenberg L C L, Klimeck G and Simmons M Y 2012 A single-atom transistor *Nature Nanotechnol.* **7** 242-6
- [27] Kurra N, Reifengerger R G and Kulkarni G U 2014 Nanocarbon-scanning probe microscopy synergy: Fundamental aspects to nanoscale devices *ACS Appl. Mater. Interfaces* **6** 6147-63
- [28] Custance O, Perez R and Morita S 2009 Atomic force microscopy as a tool for atom manipulation *Nature Nanotechnol.* **4** 803-10
- [29] Garcia R, Knoll A W and Riedo E 2014 Advanced scanning probe lithography *Nature Nanotechnol.* **9** 577-87
- [30] Thundat T, Nagahara L A, Oden P I, Lindsay S M, George M A, and Glaunsinger W S 1990 Modification of tantalum surfaces by scanning tunneling microscopy in an electrochemical cell *J. Vac. Sci. Technol. A* **8** 3537-41
- [31] Xie X N, Chung H J, Sow C H and Wee A T S 2006 Nanoscale materials patterning and engineering by atomic force microscopy nanolithography *Mat. Sci. Eng. R* **54** 1-48

- [32] Kalff F E, Rebergen M P, Fahrenfort E, Girovsky J, Toskovic R, Lado J L, Fernández – Rossier J and Otte A F 2016 A kilobyte rewritable atomic memory *Nat. Nanotechnol.* (Advanced online publication doi 10.1038/nnano.2016.131)
- [33] Day H C and Allee D R 1993 Selective area oxidation of silicon with a scanning force microscope *Appl. Phys. Lett.* **62** 2691-3
- [34] Snow E S and Campbell P M 1994 Fabrication of Si nanostructures with an atomic force microscope *Appl. Phys. Lett.* **64** 1932-4
- [35] Pérez-Murano F, Abadal G, Barniol N, Aymerich X, Servat J, Gorostiza P and Sanz F 1995 Nanometer-scale oxidation of Si (100) surfaces by tapping mode atomic-force microscopy *J. Appl. Phys.* **78** 6797 - 801
- [36] Garcia R and San Paulo A 1999 Attractive and repulsive tip-sample interaction regimes in tapping-mode atomic force microscopy *Phys. Rev. B* **60** 4961-7
- [37] Garcia R, Calleja M and Pérez-Murano F 1998 Local oxidation of silicon surfaces by dynamic force microscopy: Nanofabrication and water bridge formation *Appl. Phys. Lett.* **72** 2295-7
- [38] Garcia R 2010 Amplitude modulation Atomic Force Microscopy First Ed. Wiley
- [39] Reifenberger R 2016 Fundamentals of atomic force microscopy. Part I: Foundations First Ed. World Scientific
- [40] Garcia R, Losilla N S, Martínez J, Martinez R V, Palomares F J, Huttel Y, Calvaresi M and Zerbetto F 2010 Nanopatterning of carbonaceous structures by field-induced carbon dioxide splitting with a force microscope *Appl. Phys. Lett.* **96** 143110.
- [41] Yang S M, Stelcov E, Paranthaman M P, Tselev A, Noh T W and Kalinin S V 2015 Humidity effect on nanoscale electrochemistry in solid silver ion conductors at the dual nature of its locality *Nano Lett.* **15** 1062-9
- [42] Yang S M, Paranthaman M P, Noh T W, Kalinin S V and Stelcov E 2016 Nanoparticle shape evolution and proximity effects during tip-induced electrochemical processes *ACS Nano* **10** 663-71
- [43] Brown B P, Picco L, Miles M J and Faul C F J 2015 Conductive-AFM patterning of organic semiconductors *Small* **11** 5054-8
- [44] Tello M, Garcia R and Martin-Gago J A 2005 Bottom-up fabrication of carbon-rich silicon carbide nanowires by manipulation of nanometer-sized ethanol menisci *Adv. Mater.* **17** 1480-3
- [45] Garcia R, Calleja M and Rohrer H 1999 Patterning of silicon surfaces by non-contact atomic force microscopy: field-induced formation of nanometer-size water bridges *J. Appl. Phys.* **86** 1898-903
- [46] Sugimura H, Uchida T, Kitamura N and Masuhara H 1994 Scanning tunneling microscope tip-induced anodization of nanofabrication of titanium *J. Phys. Chem.* **98**, 4352-4357.
- [47] Gomez-Moñivas S, Saenz J J, Calleja M and Garcia R 2003 Field-induced formation of nanometer-sized water bridges *Phys. Rev. Lett.* **91** 056101

- [48] Garcia-Martin A and Garcia R 2006 Formation of nanoscale liquid menisci in electric fields *Appl. Phys. Lett.* **88** 123115
- [49] Bard A J and Mirkin M V 2012 Scanning electrochemical microscopy 2<sup>nd</sup> Ed. CRC Press
- [50] Calleja M, Tello M and Garcia R 2002 Size determination of field-induced water menisci in noncontact atomic force microscopy *J. Appl. Phys.* **92** 5539-42
- [51] Djurkovic S, Clemons C B, Golovaty D and Young G W 2007 Effects of the electric field shape on nano-scale oxidation *Surf. Sci.* **601** 5340-58
- [52] Cramer T, Zerbetto F and Garcia R 2008 Molecular mechanism of water bridge buildup: Field-induced formation of nanoscale menisci *Langmuir* **24** 6116-20
- [53] Vicary J A and Miles M J 2009 Real-time nanofabrication with high-speed atomic force microscopy *Nanotechnology* **20** 095302
- [54] Angelov T, Roeser D, Ivanov T, Gutschmidt S, Sattel T and Rangelow I W 2016 Thermo-mechanical transduction suitable for high-speed scanning probe imaging and lithography *Microelectron. Eng.* **154** 1-7
- [55] Kinser C R, Schmitz M J and Hersam M C 2006 Kinetics and mechanism of atomic force microscope local oxidation on hydrogen-passivated silicon in inert organic solvents *Adv. Mater.* **18** 1377-80
- [56] Dubois E and Bubendorff J L 2000 Kinetics of scanned probe oxidation: space-charge limited growth *J. Appl. Phys.* **87** 8148-54
- [57] Calleja M and Garcia R 2000 Nano-oxidation of silicon surfaces by noncontact atomic force microscopy: size dependence on voltage and pulse duration *Appl. Phys. Lett.* **76** 3427-9
- [58] Dagata J, Pérez-Murano F, Martin C, Kuramochi H and Yokoyama H 2004 Current, charge, and capacitance during scanning probe oxidation of silicon I: Maximum charge density and lateral diffusion *J. Appl. Phys.* **96** 2386-92
- [59] Chiesa M and Garcia R 2010 Nanoscale space charge generation in local oxidation nanolithography *Appl. Phys. Lett.* **96** 263112
- [60] Baumgärtel T, Borczykowski C V and Graaf H 2012 Detection and stability of nanoscale space charges in local oxidation nanolithography *Nanotechnology* **23** 095707
- [61] Kuramochi H and Dagata J A 2011 Local oxidation using dynamic force mode: Toward higher reliability and efficiency. Chapter 2 in book: Tip-based nanofabrication. Fundamental and applications Tseng, A. A. (Ed.) First Ed. Springer 65-90
- [62] Dagata J A, Inoue T, Itoh J, Matsumoto K and Yokoyama H 1998 Role of space charge in scanned probe oxidation *J. Appl. Phys.* **84** 6891-6900
- [63] Pérez-Murano F, Birkelund K, Morimoto K and Dagata J A 1999 Voltage modulation scanning probe oxidation *Appl. Phys. Lett.* **75** 199-201
- [64] Avouris P, Hertel T and Martel R 1997 Atomic force microscope tip-induced local oxidation of silicon: Kinetics, mechanism, and nanofabrication *Appl. Phys. Lett.* **71** 285-7
- [65] Kuramochi H, Pérez-Murano F, Dagata J A and Yokoyama H 2004 Faradaic current detection during anodic oxidation of the H-passivated p-Si(001) surface with controlled relative humidity *Nanotechnology* **15** 297-302



- [66] Fontaine P A; Dubois E and Stiévenard D 1998 Characterization of scanning tunneling microscopy and atomic force microscopy-based techniques for nanolithography on hydrogen-passivated silicon *J. Appl. Phys.* **84** 1776-81
- [67] Ulrich A J and Radadia A D 2015 Conductive polycrystalline diamond probes for local anodic oxidation lithography *Nanotechnology* **26** 465201
- [68] Cooper E B, Manalis S R, Fang H, Dai H, Matsumoto K, Minne S C, Hunt T and Quate C F 1999 Terabit-per-square-inch data storage with the atomic force microscope *Appl. Phys. Lett.* **75** 3566-8
- [69] Rius G, Lorenzoni M, Matsui S, Tanemura M and Perez-Murano F 2015 Boosting the local anodic oxidation of silicon through carbon nanofiber atomic force microscopy probes *Beilstein J. Nanotechnol.* **6** 215-222
- [70] Tello M and Garcia R 2001 Nano-oxidation of silicon surfaces: Comparison of noncontact and contact AFM methods *Appl. Phys. Lett.* **79** 424-6
- [71] Gasser U, Sigrüst M, Gustavsson S, Ensslin K and Ihn T 2011 Double layer local anodic oxidation using atomic force microscopy Chapter 3 in book: Tip-based nanofabrication. Fundamental and applications Tseng, A. A. (Ed.) First Ed. Springer 91-127
- [72] Lazzarino M, Heun S, Ressel B, Prince K C, Pingue P and Ascoli C 2002 Atomic force microscope anodic oxidation studied by spectroscopy microscopy *Appl. Phys. Lett.* **81** 2842-4
- [73] Pavlova A Y, Nikulin Y V, Dzhumaliev A S, Khivintsev Y V, Zaharov A A, Preobrazhensky V L, Pernod P and Filimonov Y A 2015 Local anodic oxidation of Ni films with (200) and (111) texture *Appl. Surf. Sci.* **347** 435-8
- [74] Buyukkose S, Okur S and Aygun G 2009 Local oxidation nanolithography on Hf thin films using atomic force microscopy (AFM) *J. Phys. D: Appl. Phys.* **42** 105302
- [75] Lorenzoni M and Torre B 2013 Scanning probe oxidation of SiC, fabrication and kinetics considerations *Appl. Phys. Lett.* **103** 163109
- [76] Chien F S S, Chou Y C, Chen T T, Hsieh W F, Chao T S and Gwo S 2001 Nano-oxidation of silicon nitride films with an atomic force microscope: Chemical mapping, kinetics, and applications *J. Appl. Phys.* **89** 2465-72
- [77] Yong G J, Vanderlinde W E, Tanyi E K, Schaefer D M, Stumpf C and Kolagani R M 2016 Possible mechanisms in atomic force microscope- induced nano-oxidation lithography in epitaxial  $\text{La}_{0.67}\text{Ba}_{0.33}\text{MnO}_{3-d}$  thin films *J. Vac. Sci. Technol. B* **34** 021601
- [78] Espinosa F M, Ryu Y K, Marinov K, Dumcenco D, Kis A and Garcia R 2015 Direct fabrication of thin layer  $\text{MoS}_2$  field-effect nanoscale transistors by oxidation scanning probe lithography *Appl. Phys. Lett.* **106** 103503
- [79] Donarelli M, Perrozzi F, Bisti F, Paparella F, Feyer V, Ponzoni A, Gonchigsuren M and Ottaviano L 2015 Few layered  $\text{MoS}_2$  lithography with an AFM tip: description of the technique and nanospectroscopy investigations *Nanoscale* **7** 11453-9
- [80] Dago A I, Ryu Y K and Garcia R 2016 Sub-20 nm patterning of thin layer  $\text{WSe}_2$  by scanning probe lithography *Appl. Phys. Lett.* **109** 163103

- [81] Pinilla-Cienfuegos E, Mañas-Valero S, Navarro-Moratalla E, Tatay S, Forment-Aliaga A and Coronado E 2016 Local oxidation nanolithography on metallic transition metal dichalcogenides surfaces *Appl. Sci.* **6** 250
- [82] Limpoco T and Proksch R (private communication), Asylum Research, Oxford Instruments.
- [83] Martinez R V, Martinez J, Chiesa M, Garcia R, Coronado E, Pinilla-Cienfuegos E and Tatay S 2010 Large-scale nanopatterning of single proteins used as carriers of magnetic nanoparticles *Adv. Mater.* **22** 588-91
- [84] Dago A I and Garcia R 2016 Quantum transport devices fabricated by oxidation scanning probe lithography *Unpublished material*
- [85] Coronado E, Forment-Aliaga A, Navarro-Moratalla E, Pinilla-Cienfuegos E and Castellanos – Gomez A 2013 Nanofabrication of TaS<sub>2</sub> conducting layers nanopatterned with Ta<sub>2</sub>O<sub>5</sub> insulating regions via AFM *J. Mater. Chem. C* **1** 7692-4
- [86] Wang P, Okamoto K and Tamada K 2014 Tuning the work functions of two-dimensional silver nanoparticle sheets using local oxidation nanolithography *Adv. Mater. Interfaces* **1** 1400268-1
- [87] Mo Y, Lu Z, Chau A and Huang F 2013 Preparation and mechanics of nanotextures on adapting a low adhesive surface using local oxidation nanolithography *ACS Appl. Mater. Interfaces* **5** 4356-60
- [88] Huang C Y, Yao Y C, Lee Y J, Lin T Y, Kao W J, Hwang J S, Yang Y J and Shen J L 2014 Local nanotip arrays sculptured by atomic force microscopy to enhance the light-output efficiency of GaN-based light-emitting diode structures *Nanotechnology* **25** 195401
- [89] Garcia R, Tello M, Moulin J F and Biscarini F 2004 Size and shape controlled growth of molecular nanostructures on silicon oxide templates *Nano Lett.* **4** 1115-9
- [90] Martinez R V, Garcia F, Garcia R, Coronado E, Forment-Aliaga A, Romero F M and Tatay S 2007 Nanoscale deposition of single-molecule magnets onto SiO<sub>2</sub> patterns *Adv. Mater.* **19** 291-5
- [91] Coronado E, Forment-Aliaga A, Pinilla-Cienfuegos E, Tatay S, Catala L and Plaza J A 2012 Nanopatterning of anionic nanoparticles based on magnetic prussian-blue analogues *Adv. Funct. Mater.* **22** 3625-33
- [92] Yoshinobu T, Suzuki J, Kurooka H, Moon W C and Iwasaki 2003 AFM fabrication of oxide patterns and immobilization of biomolecules on Si surface *Electrochim. Acta* **48** 3131-5
- [93] Qin G, Gu J, Liu K, Xiao Z, Yam C M and Cai C 2011 Conductive AFM patterning on oligo (ethylene glycol)-terminated alkyl monolayers on silicon substrates: proposed mechanism and fabrication of avidin patterns *Langmuir* **27** 6987-94
- [94] Baumgartel T, Rehm S, Wurthner F, Borczykowski C von and Graaf H 2014 Functional bismide dyes bound via electrostatic interactions to oxide nanostructures generated by AFM lithography *Appl. Surf. Sci.* **318** 51-8
- [95] Fernández-Regúlez M, Evangelio L, Lorenzoni M, Fraxedas J and Pérez-Murano F 2014 Sub-10 nm resistless nanolithography for directed self-assembly of block copolymers *ACS Appl. Mater. Interfaces* **6** 21596-602

- [96] Maoz R, Cohen S R, and Sagiv J 1999 Nanoelectrochemical patterning of monolayer surfaces: toward spatially defined self-assembly of nanostructures *Adv. Mater.* **11** 55-61
- [97] Sugimura H, Hanji T, Hayashi K and Takai O 2002 Surface potential nanopatterning combining alkyl and fluoroalkylsilane self-assembled monolayers fabricated via scanning probe lithography *Adv. Mater.* **14** 524-6
- [98] Lee W, Kim E R and Lee H 2002 Chemical approach to high-resolution patterning on self-assembled monolayers using atomic force microscope lithography *Langmuir* **18** 8375-80
- [99] Benetti E M, Chung H J and Vancso G J 2009 pH response polymeric brush nanostructures: Preparation and characterization by scanning probe oxidation and surface initiated polymerization *Macromol. Rapid Comm.* **30** 411-7
- [100] Liu S, Maoz R and Sagiv J 2004 Planned nanostructures of colloidal gold via self-assembly on hierarchically assembled organic bilayer template patterns with in-situ generated terminal amino functionality *Nano Lett.* **4** 845-51
- [101] Kwon G, Chu H, Yoo J, Kim H, Han C, Chung C, Lee J and Lee H 2012 Fabrication of uniform and high resolution copper nanowire using intermediate self-assembled monolayers through direct AFM lithography *Nanotechnology* **23** 185307
- [102] Germain J, Rolandi M, Backer S A and Fréchet M J 2008 Sulfur as a novel nanopatterning material: An ultrathin resist and a chemically addressable template for nanocrystal self-assembly *Adv. Mater.* **20** 4526-9
- [103] Yang J, Ichii T, Murase K and Sugimura H 2012 Site-selective assembly and reorganization of gold nanoparticles along aminosilane-covered nanolines prepared on Indium-Tin oxide *Langmuir* **28** 7579-84
- [104] Berson J, Zeira A, Maoz R, and Sagiv J 2012 Parallel- and serial-contact electrochemical metallization of monolayer nanopatterns: a versatile synthetic tool en route to bottom-up assembly of electric nanocircuits *Beilstein J. Nanotechnol.* **3** 134-43
- [105] Maoz R, Frydman E, Cohen S R and Sagiv J 2000 "Constructive nanolithography": Inert monolayers as patternable templates for in-situ nanofabrication of metal-semiconductor-organic surface structures - A generic approach. *Adv. Mater.* **12** 725-31
- [106] Druzhinina T S, Hoepfener S and Schubert U S 2012 New design concepts for the fabrication of nanometric gap structures: electrochemical oxidation of OTS mono- and bilayer structures *Small* **6** 852-7
- [107] Druzhinina T S, Höpfener C, Hoepfener S and Schubert U S 2013 Hierarchical, guided self-assembly of preselected carbon nanotubes for the controlled fabrication of CNT structures by electrooxidative nanolithography *Langmuir* **29** 7515-20
- [108] Wouters D, Willems R, Hoepfener S, Flipse C F J and Schubert U S 2005 Oxidation conditions for octadecyl trichlorosilane monolayers on silicon: A detailed atomic force microscopy study of the effects of pulse height and duration on the oxidation of the monolayer and the underlying Si substrate *Adv. Func. Mater.* **15** 938-44
- [109] Druzhinina T, Hoepfener S, Herzer N and Schubert U S 2011 Fabrication of ring structures by anodization lithography on self-assembled OTS monolayers *J. Mater. Chem.* **21** 8532-6

- [110] Martin-Sanchez J, Gonzalez Y, Gonzalez L, Tello M, Garcia R, Granados D, Garcia J M and Briones F 2005 Ordered InAs quantum dots on pre-patterned GaAs (001) by local oxidation nanolithography *J. Cryst. Growth* **284** 313-8
- [111] Herranz J, Gonzalez L, Wewior L, Alen B, Fuster D and Gonzalez Y 2015 Study of growth parameters for single InAs QD formation on GaAs (001) patterned substrates by local oxidation lithography *Crys. Growth Des.* **15** 666-72
- [112] Mukai K, Hirota A and Nakashima S 2015 Position control of PbS quantum dot using nanohole on silicon substrate processed by scanning probe lithography *Jpn. J. Appl. Phys.* **54** 04DJ02
- [113] Kim H C, Park S M and Hinsberg W D 2010 Block copolymer based nanostructures: Materials, processes and application to electronics *Chem. Rev.* **110** 146-177
- [114] Sigrist M, Fuhrer A, Ihn T, Ensslin K, Driscoll D C and Gossard A C 2004 Multiple layer local oxidation for fabricating semiconductor nanostructures *Appl. Phys. Lett.* **85** 3558-60
- [115] Matsumoto K, Gotoh Y, Maeda T, Dagata J A and Harris J S 2000 Room-temperature single-electron memory made by pulse-mode atomic force microscopy nano oxidation process on atomically flat  $\alpha$ -alumina substrate *Appl. Phys. Lett.* **76** 239-41
- [116] Snow E S and Campbell P M 1995 AFM fabrication of sub-10-nanometer metal-oxide devices with in situ control of electric properties *Science* **270** 1639-41
- [117] Ryu Y K, Postigo P A, Garcia F and Garcia R 2014 Fabrication of sub-12 nm thick silicon nanowires by processing scanning probe lithography masks *Appl. Phys. Lett.* **104** 223112
- [118] Campbell P M, Snow E S and McMarr P J 1995 Fabrication of nanometer-scale side-gated silicon field-effect transistors with an atomic-force microscope *Appl. Phys. Lett.* **66** 1388-90
- [119] Minne S C, Soh H T, Flueckiger Ph and Quate C F 1995 Fabrication of 0.1  $\mu\text{m}$  metal-oxide-semiconductor field-effect transistors with the atomic-force microscope *Appl. Phys. Lett.* **66** 703-5
- [120] Clement N, Tonneau D, Dallaporta H, Bouchiat V, Fraboulet D, Mariole D, Gautier J and Safarov V 2002 Electronic transport properties of single-crystal silicon nanowires fabricated using an atomic force microscope *Physica E* **13** 999-1002
- [121] Martinez J, Martinez R V and Garcia R 2008 Silicon nanowire transistors with a channel width of 4 nm fabricated by atomic force microscope nanolithography *Nano Lett.* **8** 3636-9
- [122] Davis Z J, Abadal G, Hansen O, Borisé X, Barniol N, Pérez-Murano F and Boisen A 2003 AFM lithography of aluminum for fabrication of nanomechanical systems *Ultramicroscopy* **97** 467-472
- [123] Pellegrino L, Yanagisawa Y, Ishikawa M, Matsumoto T, Tanaka H and Kawai T 2006 (Fe,Mn)<sub>3</sub>O<sub>4</sub> nanochannels fabricated by AFM local-oxidation nanolithography using Mo/poly(methylmethacrylate) nanomasks *Adv. Mater.* **18** 3099-3104
- [124] Gotoh Y, Matsumoto K, Maeda T, Cooper E B, Manalis S R, Fang H, Minne S C, Hunt T, Dai H, Harris J and Quate C F 2000 Experimental and theoretical results of room-temperature single-electron transistor formed by atomic force microscope nano-oxidation process *J. Vac. Sci. Technol. A* **18** 1321-5

- [125] Arai M, Masubuchi S, Nose K, Mitsuda Y and Machida T 2015 Fabrication of 10-nm-scale nanoconstrictions in graphene using atomic force microscopy-based local anodic oxidation lithography *Jpn. J. Appl. Phys.* **54** 04DJ06
- [126] Shirakashi, J I and Takemura, Y 2004 Ferromagnetic ultra-small tunnel junction devices fabricated by scanning probe microscope (SPM) local oxidation *IEEE T. Magn.* **40** 2640-2
- [127] Ryu Y K, Chiesa M and Garcia R 2013 Electric characteristics of silicon nanowire transistors fabricated by scanning probe and electron beam lithographies *Nanotechnology* **24** 315205-1
- [128] Chiesa M, Cardenas P P, Oton F, Martinez J, Mas-Torrent M, Garcia F, Alonso J C, Rovira C and Garcia R 2012 Detection of the early stage of recombinational DNA repair by silicon nanowire transistors *Nano Lett.* **12** 1275-81
- [129] Weng L, Zhang L, Chen Y P and Rokhinson L P 2008 Atomic force microscope local oxidation lithography of graphene *Appl. Phys. Lett.* **93** 093107
- [130] Neubeck S, Ponomarenko L A, Freitag F, Giesbers A J M, Zeitler U, Morozov S V, Blake P, Geim A K and Novoselov K S 2010 From one electron to one hole: quasiparticle counting in graphene quantum dots determined by electrochemical and plasma etching *Small* **6** 1469-73
- [131] Puddy R K, Chua C J and Buitelaar M R 2013 Transport spectroscopy of a graphene quantum dot fabricated by atomic force microscope nanolithography *Appl. Phys. Lett.* **103** 183117
- [132] Lee D H, Kim C K, Lee J H, Chung H J and Park B H 2016 Fabricating in-plane transistor and memory using atomic force microscope lithography towards graphene system on chip *Carbon* **96** 223-8
- [133] Masubuchi S, Arai M and Machida T 2011 Atomic force microscopy based tunable local anodic oxidation of graphene *Nano Lett.* **11** 4542-6
- [134] Berson J, Burshtain D, Zeira A, Yoffe A, Maoz R and Sagiv J 2015 Single-layer ionic conduction on carboxyl-terminated silane monolayers patterned by constructive lithography *Nat. Mater.* **14** 613-21
- [135] Komijani Y, Csontos M, Ihn T, Ensslin K, Meir Y, Reuter D and Wieck A D 2013 Origins of conductance anomalies in a p-type GaAs quantum point contact *Phys. Rev. B* **87** 245406
- [136] Fuhrer A, Lüscher S, Ihn T, Heinzl T, Ensslin K, Wegscheider W and Bichler M 2001 Energy spectra of quantum rings *Nature* **413** 822-5
- [137] Heine A W, Tutuc D, Zwicknagl G and Haug R J 2016 Competition between Kondo screening and quantum Hall edge reconstruction *Phys. Rev. Lett.* **116** 096802
- [138] Ubbelohde N, Fricke C, Hohls F and Haug R J 2013 Spin-dependent shot noise enhancement in a quantum dot *Phys. Rev. B* **88** 041304 (R)
- [139] Rogge M C, Räsänen E and Haug R J 2010 Interaction-induced spin polarization in quantum dots *Phys. Rev. Lett.* **105** 046802
- [140] Delacour C, Pannetier B, Villegier J C and Bouchiat V 2012 Quantum and thermal phase slips in superconducting niobium nitride (NbN) ultrathin crystalline nanowire: Application to single photon detection *Nano Lett.* **12** 3501-6

- [141] Hong L Y and Lin H N 2015 Fabrication of single titanium oxide nanodot ultraviolet sensors by atomic microscopy nanolithography *Sensor. Actuat. A-Phys.* **232** 94-8
- [142] Yokoo A, Tanabe T, Kuramochi E and Notomi M 2011 Ultrahigh-Q nanocavities written with a nanoprobe *Nano Lett.* **11** 3634-42
- [143] Lee N, Jo W, Liu C and Mény C 2014 Size dependent bipolar resistance switching of NiO nanodots for low-power and multi-state operation *Nanotechnology* **25** 415302
- [144] Takemura Y and Shirakashi J I 2005 Modification of electric properties and magnetic domain structures in magnetic nanostructures by AFM nanolithography *Adv. Engineering Mater.* **7** 170-3
- [145] Cavallini M, Hemmatian Z, Riminucci A, Prezioso M, Morandi V and Murgia M 2012 Regenable resistive switching in silicon oxide based nanojunctions *Adv. Mater.* **24** 1197-201
- [146] Cavallini M *et al* 2010 Additive nanoscale embedding of functional nanoparticles on silicon surface *Nanoscale* **2** 2069-72
- [147] Lavini F *et al* 2015 Bias assisted scanning probe microscopy direct write lithography enables local oxygen enrichment of lanthanum cuprates thin films *Nanotechnology* **26** 325302
- [148] Martín-Sánchez J, Muñoz-Matutano G, Herranz J, Canet-Ferrer J, Alén B, González Y, Alonso-González P, Fuster D, González L, Martínez-Pastor J and Briones F 2009 Single Photon Emission from Site-Controlled InAs Quantum Dots Grown on GaAs(001) Patterned Substrates *ACS Nano* **3** 1513-7
- [149] Byun I S *et al* 2011 Nanoscale lithography on monolayer graphene using hydrogenation and oxidation *ACS Nano* **5** 6417-24
- [150] Lorenzoni M, Giugni A and Torre B 2013 Oxidative and carbonaceous patterning of Si surface in an organic media by scanning probe lithography *Nanoscale Res. Lett.* **8**:75
- [151] Martínez R V and Garcia R 2005 Nanolithography based on the formation and manipulation of nanometer-size organic liquid menisci *Nano Lett.* **5** 1161-4
- [152] Marchi F, Bouchiat H, Dallaporta V, Safarov V, Tonneau D and Doppett P 1998 Growth of silicon oxide on hydrogenated silicon during lithography with an atomic force microscope *J. Vac. Sci. Technol. B* **16** 2952-6
- [153] Maoz R, Burshtain D, Cohen H, Nelson P, Berson J, Yoffe A and Sagiv J 2016 Site-targeted interfacial solid-phase chemistry: Surface functionalization of organic monolayers via chemical transformations locally induced at the boundary between two solids *Angew. Chem. Int. Ed.* **55**, 12366-71
- [154] Calvaresi M., Martinez R V , Losilla N S., Martinez J, Garcia R and Zerbetto F 2010 Splitting CO<sub>2</sub> with electric fields: A computational investigation, *J. Phys. Chem. Lett.* **1**, 3256-3260.
- [155] Minne S C, Adams J D, Yaralioglu G, Manalis, S.R., Atalar, A and Quate, C F 1998. Centimeter scale atomic force microscope imaging and lithography, *Appl. Phys. Lett.* **73**, 1742-1744.
- [156] Hoepfner S, Maoz R and Sagiv J 2003 Constructive microlithography: Electrochemical printing of monolayer template patterns extends constructive nanolithography to the micrometer-millimeter dimension range *Nano Lett.* **3** 761-7

- [157] Cavallini M., Mei P, Biscarini F and Garcia R 2003 Parallel writing by local oxidation nanolithography with submicrometer resolution *Appl. Phys. Lett.* **83** 5286-8
- [158] Albonetti C, Martinez J, Losilla N S, Greco P, Cavallini M, Borgatti F, Montecchi M, Pasquali L, Garcia R and Biscarini F 2008 Parallel-local anodic oxidation of silicon surfaces by soft stamps *Nanotechnology* **19** 434303
- [159] Losilla N S, Martinez J and Garcia R 2009 Large area nanoscale patterning of silicon surfaces by parallel local oxidation *Nanotechnology* **20** 475304.
- [160] Losilla N S, Martinez J, Bystrenova E, Greco P, Biscarini F and Garcia R 2010 Patterning pentacene surfaces by local oxidation nanolithography, *Ultramicroscopy* **110** 729-732
- [161] Zeira A, Chowdhury D, Maoz R and Sagiv J 2008 Contact Electrochemical Replication of Hydrophilic-Hydrophobic Monolayer Patterns *ACS Nano* **2** 2554–68
- [162] Simeone F C, Albonetti C and Cavallini M 2009 Progress in micro- and nanopatterning via electrochemical lithography *J. Phys. Chem. C* **113** 18987-94